

[C₆F₅Xe]⁺ and [C₆F₅XeNCCH₃]⁺ Salts of the Weakly Coordinating Borate Anions, [BY₄][−] (Y = CN, CF₃, or C₆F₅)

Karsten Koppe,^{†,‡} Hermann-J. Frohn,^{*,†} Hélène P. A. Mercier,[‡] and Gary J. Schrobilgen^{*,‡}

Anorganische Chemie, Universität Duisburg-Essen, Lotharstrasse 1, D-47048 Duisburg, Germany, and Department of Chemistry, McMaster University, Hamilton, Ontario L8S 4M1, Canada

Received November 16, 2007

New examples of [C₆F₅Xe]⁺ salts of the weakly coordinating [BY₄][−] (Y = CN, CF₃, or C₆F₅) anions were synthesized by metathesis of [C₆F₅Xe][BF₄] with M'[BY₄] (M' = K or Cs; Y = CN, CF₃, or C₆F₅) in CH₃CN at −40 °C, and were crystallized from CH₂Cl₂ or from a CH₂Cl₂/CH₃CN solvent mixture. The low-temperature (−173 °C) X-ray crystal structures of the [C₆F₅Xe]⁺ cation and of the [C₆F₅XeNCCH₃]⁺ adduct-cation are reported for [C₆F₅Xe][B(CF₃)₄], [C₆F₅XeNCCH₃][B(CF₃)₄], [C₆F₅Xe][B(CN)₄], and [C₆F₅XeNCCH₃][B(C₆F₅)₄]. The [C₆F₅Xe]⁺ cation, in each structure, interacts with either the anion or the solvent, with the weakest cation–anion interactions occurring for the [B(CF₃)₄][−] anion. The solid-state Raman spectra of the [C₆F₅Xe]⁺ and [C₆F₅XeNCCH₃]⁺ salts have been assigned with the aid of electronic structure calculations. Gas-phase thermodynamic calculations show that the donor–acceptor bond dissociation energy of [C₆F₅XeNCCH₃]⁺ is approximately half that of [FXeNCCH₃]⁺. Coordination of CH₃CN to [C₆F₅Xe]⁺ is correlated with changes in the partial charges on mainly Xe, the *ipso*-C, and N, that is, the partial charge on Xe increases and those on the *ipso*-C and N decrease upon coordination, typifying a transition from a 2c–2e to a 3c–4e bond.

Introduction

The [C₆F₅Xe]⁺ cation has been a subject of interest since its discovery in 1989.^{1–3} Although the prior characterization of [C₆F₅Xe]⁺ has included the X-ray crystal structure determinations of several of its salts, none of the structures have provided a well-isolated [C₆F₅Xe]⁺ cation. In [C₆F₅Xe][AsF₆],⁴ there is a close contact to one fluorine (2.672(5) Å) of the anion. The [C₆F₅XeNCCH₃][(C₆F₅)₂BF₂] (2.681(8) Å)³ and [C₆F₅XeNC₅H₃F₂][AsF₆] (2.694(5) Å)⁵ salts contain [C₆F₅Xe]⁺ cations that are weakly coordinated to nitrogen bases, whereas in C₆F₅XeOC(O)C₆F₅, the Xe---O interaction is significantly stronger (2.367(3) Å).^{6,7}

The syntheses of several new salts of the [C₆F₅Xe]⁺ cation, namely, those of the [B(CF₃)₄][−], [B(CN)₄][−], and [B(OTeF₅)₄][−] anions, as well as the [B(CF₃)₄][−] and [B(C₆F₅)₄][−] salts of the [C₆F₅XeNCCH₃]⁺ cation, have recently been described along with their solution characterizations by multi-NMR spectroscopy, stabilities, and reactivities.⁸ The ability of the [C₆F₅Xe]⁺ cations of the [B(CF₃)₄][−] and [B(C₆F₅)₄][−] salts to coordinate CH₃CN to xenon is primarily a consequence of the weakly coordinating natures of these anions. The use of very weakly coordinating anions suggested that it may be possible to isolate and characterize the [C₆F₅Xe]⁺ cation in a solid-state environment that more closely resembles the gas-phase cation, provided a suitable weakly coordinating solvent is used for synthesis and crystallization. The present paper reports the solid-state structural characterizations of [C₆F₅Xe][BY₄] (Y = CF₃ or CN) and [C₆F₅XeNCCH₃][BY₄] (Y = CF₃ or C₆F₅) by low-temperature X-ray crystallography and Raman spectroscopy and electronic structure calculations of the gas-phase [C₆F₅Xe]⁺ and [C₆F₅XeNCCH₃]⁺ cations,

* To whom correspondence should be addressed. E-mail: h-j.frohn@uni-due.de (H.-J.F.); schrobil@mcmaster.ca (G.J.S).

[†] Universität Duisburg-Essen.

[‡] McMaster University.

- (1) Naumann, D.; Tyrra, W. *J. Chem. Soc., Chem. Commun.* **1989**, 47–50.
- (2) Frohn, H.-J.; Jakobs, S. *J. Chem. Soc., Chem. Commun.* **1989**, 625–627.
- (3) Frohn, H.-J.; Jakobs, S.; Henkel, G. *Angew. Chem., Int. Ed. Engl.* **1989**, 28, 1506–1507.; *Angew. Chem.* **1989**, 101, 1534–1536.
- (4) Frohn, H.-J.; Klose, A.; Schroer, T.; Henkel, G.; Buss, V.; Opitz, D.; Vahrenhorst, R. *Inorg. Chem.* **1998**, 37, 4884–4890.
- (5) Frohn, H.-J.; Schroer, T.; Henkel, G. *Z. Naturforsch.* **1995**, 50b, 1799–1810.

(6) Frohn, H.-J.; Klose, A.; Henkel, G. *GIT Fachz. Lab.* **1993**, 752–755.

(7) Frohn, H.-J.; Klose, A.; Henkel, G. *Angew. Chem., Int. Ed. Engl.* **1993**, 32, 99–100.; *Angew. Chem.* **1993**, 105, 114–115.

(8) Koppe, K.; Bilir, V.; Frohn, H.-J.; Mercier, H. P. A.; Schrobilgen, G. J. *Inorg. Chem.* **2007**, 46, 9425–9437.

Table 1. Crystallographic Data for [C₆F₅XeNCCH₃][B(CF₃)₄], [C₆F₅Xe][B(CF₃)₄], [C₆F₅XeNCCH₃][B(C₆F₅)₄], and [C₆F₅XeNCCH₃][B(CN)₄]

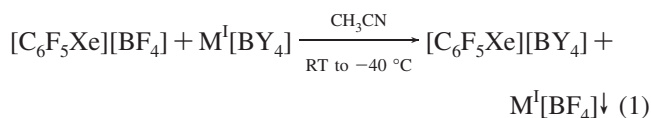
	[C ₆ F ₅ XeNCCH ₃][B(CF ₃) ₄]	[C ₆ F ₅ Xe][B(CF ₃) ₄]	[C ₆ F ₅ XeNCCH ₃][B(C ₆ F ₅) ₄]	[C ₆ F ₅ Xe][B(CN) ₄]
chemical formula	C ₁₂ H ₃ F ₁₇ BNXe	C ₁₀ F ₁₇ BXe	C ₃₂ F ₂₅ H ₃ BNXe	C ₁₀ F ₅ BN ₄ Xe
space group	<i>Pca</i> 2 ₁	<i>P2</i> ₁ / <i>c</i>	<i>P2</i> ₁ / <i>c</i>	<i>Pbca</i>
<i>a</i> (Å)	18.903(8)	6.751(2)	10.606(2)	9.919(2)
<i>b</i> (Å)	7.472(4)	15.950(5)	22.458(4)	16.269(4)
<i>c</i> (Å)	12.801(6)	14.715(4)	13.835(2)	16.783(4)
α (deg)	90	90	90	90
β (deg)	90	99.740(5)	94.775(5)	90
γ (deg)	90	90	90	90
<i>V</i> (Å ³)	1808(2)	1561.5(8)	3284(1)	2708(2)
molecules/unit cell	4	4	4	8
mol wt (g mol ⁻¹)	2505.06	2340.84	4073.86	3306.00
calcd density (g cm ⁻³)	2.284	2.489	2.060	2.027
<i>T</i> (°C)	-173	-173	-173	-173
μ (mm ⁻¹)	2.08	2.39	1.22	2.60
<i>R</i> ₁ ^a	0.0356	0.0439	0.0569	0.0364
<i>R</i> ₂ ^b	0.0469	0.0938	0.1239	0.0481

^a *R*₁ is defined as $\sum |F_o| - |F_c| / \sum |F_o|$ for $I > 2\sigma(I)$. ^b *R*₂ is defined as $[\sum (w(F_o^2 - F_c^2)^2) / \sum w(F_o^2)^2]^{1/2}$ for $I > 2\sigma(I)$.

which are compared with the solid-state geometries and are used to assist in the assignments of their vibrational frequencies.

Results and Discussion

Preparation of [C₆F₅Xe]⁺ Salts. The syntheses of [C₆F₅Xe][B(CF₃)₄], [C₆F₅Xe][B(CN)₄], [C₆F₅XeNCCH₃][B(CF₃)₄], and [C₆F₅XeNCCH₃][B(C₆F₅)₄] were achieved in nearly quantitative yields and in high purities by metatheses of [C₆F₅Xe][BF₄] with the corresponding M^I[BY₄] (Y = CF₃, CN, or C₆F₅; M^I = K or Cs) salts in CH₃CN at -40 °C (eq 1). Acetonitrile is the preferred solvent for the metatheses



because M^I[BF₄] salts have low room-temperature solubilities (5 mmol L⁻¹; negligible at -40 °C) and because [C₆F₅Xe][BY₄] (Y = CF₃, CN, or C₆F₅) and [C₆F₅Xe][BF₄] have high solubilities even at -40 °C. Minor amounts of M^I[BF₄] contaminants were avoided at -40 °C when the metatheses were carried out at high concentrations (1–1.5 mol L⁻¹) which render M^I[BF₄] essentially insoluble. Detailed synthetic descriptions are provided in ref 8.

X-ray Crystal Structures of [C₆F₅Xe][B(CF₃)₄], [C₆F₅Xe][B(CN)₄], [C₆F₅XeNCCH₃][B(CF₃)₄], and [C₆F₅XeNCCH₃][B(C₆F₅)₄]. Summaries of the refinement results and other crystallographic information are provided in Table 1. Important bond lengths and bond angles are listed in Table 2 along with calculated values.

The crystal structures of the [B(CF₃)₄]⁻⁹ and [B(C₆F₅)₄]⁻¹⁰ anions have been determined in their respective Cs⁺ and [H(OEt)₂]⁺ salts and that of the [B(CN)₄]⁻ anion has been determined in M[B(CN)₄] (M = Li, Na, Cu, Rb, Cs, [NH₄], and Tl;¹¹ Ag, K, [N(C₄H₉)₄];¹² and [P(C₆H₅)₄]).¹³ The structural parameters obtained for the [B(CF₃)₄]⁻ (Figures 1 and 2) and [B(C₆F₅)₄]⁻ (Figure 3)

anions in this study are in good agreement with the published parameters and require no further comment.

The geometrical parameters obtained for the [B(CN)₄]⁻ anion in the present study are in good agreement with the literature values; however, the closest contact distance between a nitrogen atom and the xenon atom in [C₆F₅Xe][B(CN)₄], 2.716(3) Å, is noteworthy (Figure 4). The latter contact is significantly less than the sum of the xenon (2.16 Å) and nitrogen (1.55 Å) van der Waals radii¹⁴ and is indicative of a significant cation–anion interaction. This interaction, however, does not significantly manifest itself in the geometry of the [B(CN)₄]⁻ anion, with the C–N bond that is involved in the contact being equal in length, within ±3σ, to the other three C–N bonds. The Raman spectrum in the CN stretching region, however, does show that the anion symmetry is lowered by coordination to the [C₆F₅Xe]⁺ cation (see Raman Spectroscopy). The B–C bond lengths and CBC bond angles are not significantly influenced by ion-pair formation and are equal within ±3σ. This is confirmed by Raman spectroscopy and is attributable to the buffer effect of the CN triple bond in the cation–anion interaction.

The Xe---N distance in [C₆F₅Xe][B(CN)₄] (2.716(3) Å) is comparable to the Xe---F bridge distances in [C₆F₅Xe][AsF₆] (2.714(5) and 2.672(5) Å).⁴ Aside from the long Xe---N contact, the anion retains its *T_d* symmetry and gives no indication that the C–N bond of the coordinated nitrogen atom is significantly elongated relative to the remaining three C–N bonds. The ion-pair interaction is apparently stronger with [AsF₆]⁻, giving rise to a longer As---F bridge bond having increased polarity, whereas the stronger and more covalent C–N bond is little affected in the [B(CN)₄]⁻ salt (vide supra). The interaction in [C₆F₅Xe][B(CF₃)₄] is even weaker with an Xe---F distance of 2.913(4) Å compared to the van der Waals sum of 3.63 Å for xenon and fluorine,¹⁴ thus providing the most weakly coordinated [C₆F₅Xe]⁺ cation documented to date.

(11) Küppers, T.; Bernhardt, E.; Willner, H.; Rohm, H. W.; Köckerling, M. *Inorg. Chem.* **2005**, *44*, 1015–1022.

(12) Bernhardt, E.; Henkel, G.; Willner, H. *Z. Anorg. Allg. Chem.* **2000**, *626*, 560–568.

(13) Finze, M.; Bernhardt, E.; Berkei, M.; Willner, H.; Hung, J.; Waymouth, R. M. *Organometallics* **2005**, *24*, 5103–5109.

(9) Bernhardt, E.; Henkel, G.; Willner, H.; Pawelke, G.; Bürger, H. *Chem.—Eur. J.* **2001**, *7*, 4696–4705.

(10) Jutzi, P.; Müller, C.; Stämmler, A.; Stämmler, H.-G. *Organometallics* **2000**, *19*, 1442–1444.

Table 2. Experimental Geometrical Parameters for $[C_6F_5Xe][B(CF_3)_4]$, $[C_6F_5XeNCCH_3][B(CF_3)_4]$, $[C_6F_5XeNCCH_3][B(C_6F_5)_4]$, and $[C_6F_5Xe][B(CN)_4]$ and Calculated Geometrical Parameters for $[C_6F_5Xe]^+$ and $[C_6F_5XeNCCH_3]^+$

					calcd ^a			
	[B(CF ₃) ₄] ⁻ salt		[B(C ₆ F ₅) ₄] ⁻ salt	[B(CN) ₄] ⁻ salt	[C ₆ F ₅ Xe] ⁺		[C ₆ F ₅ XeNCCH ₃] ⁺	
	[C ₆ F ₅ Xe] ⁺	[C ₆ F ₅ XeNCCH ₃] ⁺	[C ₆ F ₅ XeNCCH ₃] ⁺	[C ₆ F ₅ Xe] ⁺	SVWN	PBE1	SVWN	PBE1
bond lengths (Å)								
Xe(1)–C(1)	2.104(5)	2.100(6)	2.100(10)	2.081(3)	2.095	2.106	2.104	2.101
C(1)–C(2)	1.361(7)	1.394(8)	1.363(14)	1.380(4)	1.380	1.384	1.379	1.384
C(2)–F(1)	1.331(6)	1.315(8)	1.353(11)	1.331(4)	1.308	1.311	1.315	1.316
C(2)–C(3)	1.373(7)	1.388(14)	1.384(15)	1.379(4)	1.387	1.388	1.385	1.386
C(3)–F(2)	1.334(6)	1.372(10)	1.328(12)	1.337(4)	1.303	1.308	1.307	1.311
C(3)–C(4)	1.377(8)	1.345(15)	1.389(15)	1.377(5)	1.391	1.392	1.389	1.391
C(4)–F(3)	1.330(7)	1.335(8)	1.351(12)	1.343(4)	1.300	1.304	1.304	1.307
C(4)–C(5)	1.369(9)	1.384(8)	1.349(15)	1.378(5)	1.391	1.392	1.389	1.391
C(5)–F(4)	1.335(6)	1.308(7)	1.346(13)	1.335(4)	1.303	1.308	1.307	1.311
C(5)–C(6)	1.362(8)	1.382(9)	1.373(15)	1.380(4)	1.387	1.388	1.385	1.386
C(6)–F(5)	1.324(6)	1.341(6)	1.336(11)	1.338(4)	1.308	1.311	1.315	1.316
C(6)–C(1)	1.384(7)	1.345(8)	1.362(14)	1.377(4)	1.380	1.384	1.379	1.384
Xe(1)---N(1)		2.640(6)	2.610(11)				2.557	2.674
N(1)–C(7)		1.095(8)	1.150(14)				1.153	1.148
C(7)–C(8)		1.478(9)	1.445(18)				1.423	1.443
Xe(1)---N(4)				2.716(3)				
Xe(1)---F(10a)	2.913(4)							
bond angles (deg)								
C(1)–Xe(1)---N(1)		174.9(2)	176.9(3)				179.9	179.98
Xe(1)---N(1)–C(7)		155.0(7)	150.3(9)				180.0	179.98
N(1)–C(7)–C(8)		177.8(9)	177.6(13)				180.0	179.97
Xe(1)–C(1)–C(2)	117.8(4)	117.8(5)	118.8(8)	119.8(2)	117.6	117.7	118.6	118.7
C(1)–C(2)–C(3)	117.9(5)	115.3(8)	119.6(10)	119.1(3)	117.1	117.2	118.6	118.5
C(1)–C(2)–F(1)	120.8(5)	121.7(7)	120.4(10)	121.4(3)	121.6	121.5	120.9	120.9
F(1)–C(2)–C(3)	121.3(5)	123.1(8)	119.9(10)	119.5(3)	121.3	121.3	120.5	120.6
C(2)–C(3)–C(4)	119.9(5)	123.2(9)	117.4(11)	119.6(3)	119.9	119.9	119.5	119.6
C(2)–C(3)–F(2)	119.5(5)	116.8(10)	119.5(11)	120.4(3)	119.8	119.8	120.3	120.1
F(2)–C(3)–C(4)	120.6(5)	120.1(10)	123.1(11)	120.0(3)	120.3	120.3	120.2	120.2
C(3)–C(4)–C(5)	120.7(6)	119.9(9)	122.2(11)	121.4(3)	121.2	121.3	121.0	121.0
C(3)–C(4)–F(3)	118.9(6)	120.3(8)	116.1(11)	119.6(3)	119.4	119.4	119.5	119.5
F(3)–C(4)–C(5)	120.4(6)	119.6(7)	121.7(10)	119.0(3)	119.4	119.4	119.5	119.5
C(4)–C(5)–C(6)	120.9(5)	118.6(7)	119.8(11)	119.1(3)	119.9	119.9	119.5	119.6
C(4)–C(5)–F(4)	119.9(6)	120.2(7)	117.8(11)	120.4(3)	120.3	120.3	120.2	120.2
F(4)–C(5)–C(6)	119.2(6)	121.1(6)	122.4(11)	120.6(3)	119.8	119.8	120.3	120.1
C(5)–C(6)–C(1)	117.1(5)	120.2(6)	118.7(11)	119.6(3)	117.1	117.2	118.6	118.5
C(5)–C(6)–F(5)	122.1(5)	120.1(6)	118.5(10)	120.4(3)	121.3	121.3	120.5	120.6
F(5)–C(6)–C(1)	120.9(5)	119.7(6)	122.8(11)	120.0(2)	121.6	121.5	120.9	120.9
C(6)–C(1)–Xe(1)	118.4(4)	119.3(5)	118.8(9)	118.9(2)	117.6	117.7	118.6	118.7
C(6)–C(1)–C(2)	123.5(6)	122.8(6)	122.1(10)	121.3(3)	124.8	124.6	122.8	122.7
[C ₆ F ₅ Xe] ⁺ [C ₆ F ₅ XeNCCH ₃] ⁺								
[B(CN) ₄] ⁻		[B(CF ₃) ₄] ⁻		[B(CF ₃) ₄] ⁻		[B(C ₆ F ₅) ₄] ⁻		
bond lengths (Å)								
B–C	1.593(5)–1.609(5)	B–C	1.590(9)–1.617(8)	B–C	1.589(10)–1.629(11)	B–C	1.649(22)–1.682(19)	
C–N	1.132(4)–1.144(4)	C–F	1.354(6)–1.372(7)	C–F	1.334(8)–1.347(9)	C–C	1.357(18)–1.407(18)	
						C–F	1.324(16)–1.389(16)	
bond angles (deg)								
C–B–C	106.8(3)–112.2(3)	C–B–C	107.5(5)–111.2(5)	C–B–C	108.4(7)–111.0(6)	C–B–C	100.7(10)–113.8(11)	
B–C–N	174.6(4)–178.3(4)	B–C–F	113.0(5)–115.1(5)	B–C–F	111.4(6)–115.7(7)	B–C–C	119.5(11)–129.2(12)	
		F–C–F	103.5(4)–105.8(5)	F–C–F	103.0(6)–106.7(6)	C–C–C	119.0(12)–126.0(13)	
						C–C–F	113.3(12)–122.6(12)	

^a Calculated using SVWN/(SDB)-cc-pVTZ and PBE1PBE/(SDB)-cc-pVTZ levels.

The geometrical parameters of the unsolvated $[C_6F_5Xe]^+$ cations and those of the nitrogen base adducts are equal, within experimental error (Table 2), and are comparable to those derived from the crystal structure of $[C_6F_5Xe][AsF_6]$.⁴ In particular, the Xe–C distances are in accord with the very similar vibrational frequencies for modes containing significant Xe–C stretching components (see Raman Spectroscopy). As expected, the Xe–C bond lengths are compa-

table to the I–C bond length in isoelectronic C_6F_5I (2.077(4) Å).¹⁵ The only prior example showing a significant Xe–C bond lengthening upon coordination of $[C_6F_5Xe]^+$ is $C_6F_5XeOC(O)C_6F_5$, with a Xe–C bond length of 2.122(4) Å.^{6,7} It is noteworthy that $[C_6F_5XeNCCH_3]^+$ salts do not, in all cases, crystallize from CH_3CN/CH_2Cl_2 solutions. Crystalline salts containing the $[AsF_6]^-$ anion that have been

(14) Bondi, A. *J. Phys. Chem.* **1964**, *68*, 441–451.

(15) Frohn, H.-J.; Görg, S.; Henkel, G.; Läge, M. *Z. Anorg. Allg. Chem.* **1995**, *621*, 1251–1256.

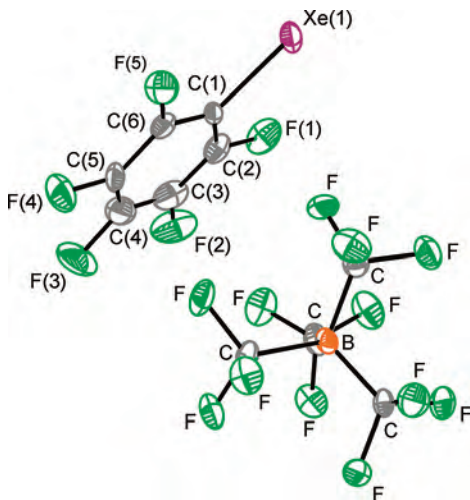


Figure 1. Crystal structure of $[\text{C}_6\text{F}_5\text{Xe}][\text{B}(\text{CF}_3)_4]$ where thermal ellipsoids are shown at the 50% probability level.

obtained from $\text{CH}_3\text{CN}/\text{CH}_2\text{Cl}_2$ solutions at $\sim 20^\circ\text{C}$ have no CH_3CN coordinated to $[\text{C}_6\text{F}_5\text{Xe}]^+$.⁴ In this instance, the $[\text{AsF}_6]^-$ anion, which is generally regarded as a weakly coordinating anion, is unexpectedly favored over CH_3CN as a coordinating base.

The geometric parameters of the $[\text{C}_6\text{F}_5\text{XeNCCH}_3]^+$ cations in the $[\text{B}(\text{CF}_3)_4]^-$ and $[\text{B}(\text{C}_6\text{F}_5)_4]^-$ salts are essentially identical to those published earlier for $[\text{C}_6\text{F}_5\text{XeNCCH}_3][(\text{C}_6\text{F}_5)_2\text{BF}_2]$.³ In all three cases, the adduct-cation is well separated from the anion. The experimental C–N bond lengths for $[\text{C}_6\text{F}_5\text{XeNCCH}_3][(\text{C}_6\text{F}_5)_2\text{BF}_2]$ (1.140(8) Å), $[\text{C}_6\text{F}_5\text{XeNCCH}_3][\text{B}(\text{CF}_3)_4]$ (1.096(9) Å), and $[\text{C}_6\text{F}_5\text{XeNCCH}_3][\text{B}(\text{C}_6\text{F}_5)_4]$ (1.157(19) Å) are equal, within $\pm 3\sigma$, to that observed in CH_3CN (1.141(2) Å).¹⁶ This is in agreement with the Raman spectra which show only a small complexation shift for the C–N stretching frequency (vide infra). This shift is much smaller for $[\text{C}_6\text{F}_5\text{XeNCCH}_3][\text{B}(\text{C}_6\text{F}_5)_4]$ (25 cm^{-1}) and $[\text{C}_6\text{F}_5\text{XeNCCH}_3][\text{B}(\text{CF}_3)_4]$ (30 cm^{-1}) than for $[\text{FXeNCCH}_3]^+$ (59 cm^{-1})¹⁷ where the C–N and Xe---N distances are 1.12(1) and 2.179(7) Å,¹⁸ respectively, and are in accord with $[\text{XeF}]^+$ being a significantly stronger Lewis acid than $[\text{C}_6\text{F}_5\text{Xe}]^+$ (see Computational Results). The C–Xe---N bond angles are 174.8(2) and 177.1(4)° in the $[\text{B}(\text{CF}_3)_4]^-$ and the $[\text{B}(\text{CN})_4]^-$ salts, respectively, and are comparable to that of the $[(\text{C}_6\text{F}_5)_2\text{BF}_2]^-$ salt (174.5(3)°). The C–Xe---N bend is assigned at 161 and 164 cm^{-1} in the $[\text{B}(\text{CF}_3)_4]^-$ and $[\text{B}(\text{C}_6\text{F}_5)_4]^-$ salts, respectively, suggesting these angles are highly deformable and that deviation from linearity in $[\text{C}_6\text{F}_5\text{XeNCCH}_3]^+$ arises from crystal packing. A similar deviation from linearity has been observed in $[\text{C}_6\text{F}_5\text{Xe}][\text{AsF}_6]$, where the C–Xe---F angles were 170.5(3) and 174.2(3)°.⁴

Raman Spectroscopy. The vibrational frequencies obtained from the low-temperature solid-state Raman spectra of $[\text{C}_6\text{F}_5\text{Xe}][\text{B}(\text{CN})_4]$, $[\text{C}_6\text{F}_5\text{XeNCCH}_3][\text{B}(\text{CF}_3)_4]$ (Figure 5),

$[\text{C}_6\text{F}_5\text{Xe}][\text{BF}_4]$, and $[\text{C}_6\text{F}_5\text{XeNCCH}_3][\text{B}(\text{C}_6\text{F}_5)_4]$ (Figure S1), and their assignments are provided in Tables 3 and 4. The frequency assignments are based on calculated gas-phase frequencies of the $[\text{C}_6\text{F}_5\text{Xe}]^+$ and $[\text{C}_6\text{F}_5\text{XeNCCH}_3]^+$ cations (see Computational Results) and prior assignments of their respective anions.

(a) $[\text{C}_6\text{F}_5\text{Xe}]^+$, $\text{C}_6\text{F}_5\text{I}$, and $[\text{C}_6\text{F}_5\text{XeNCCH}_3]^+$. There are no published vibrational frequency assignments for the $[\text{C}_6\text{F}_5\text{Xe}]^+$ or $[\text{C}_6\text{F}_5\text{XeNCCH}_3]^+$ cations, and only unassigned infrared frequencies have been provided for $\text{C}_6\text{F}_5\text{XeOC}(\text{O})\text{C}_6\text{F}_5$ ^{6,7} and $[\text{C}_6\text{F}_5\text{XeNCCH}_3][(\text{C}_6\text{F}_5)_2\text{BF}_2]$.³ The frequency assignments for $[\text{C}_6\text{F}_5\text{Xe}]^+$ and $[\text{C}_6\text{F}_5\text{XeNCCH}_3]^+$ were made by comparison with the calculated frequencies and Raman intensities (Tables 3 and 4) of the energy-minimized geometries (Figures 2 and 4) and, in the case of CH_3CN modes, by comparison with those of the free ligand and other CH_3CN adducts.¹⁸ The geometries and frequencies of $\text{C}_6\text{F}_5\text{H}$, $\text{C}_6\text{F}_5\text{Br}$, $\text{C}_6\text{F}_5\text{Cl}$, C_6F_6 , and isoelectronic $\text{C}_6\text{F}_5\text{I}$ were also calculated using the same methods and basis sets (Tables S1–S3), allowing comparisons to be made based on the new assignments.

There is overall good agreement between the observed and calculated frequencies for $[\text{C}_6\text{F}_5\text{Xe}]^+$, $[\text{C}_6\text{F}_5\text{XeNCCH}_3]^+$, and $\text{C}_6\text{F}_5\text{I}$, with slightly better agreement for the PBE1PBE values, given in square brackets, below 900 cm^{-1} . The bands assigned to C_6F_5 -ring modes are comparable to those observed in other systems containing C_6F_5 groups, for example, $\text{C}_6\text{F}_5\text{H}$,²⁰ C_6F_6 ,²¹ $\text{C}_6\text{F}_5\text{Cl}$,^{22–24} and $\text{C}_6\text{F}_5\text{Br}$.^{22–24}

The bands at 795 ($[\text{BF}_4]^-$), 794 ($[\text{B}(\text{CN})_4]^-$), and 805 ($\text{C}_6\text{F}_5\text{I}$) cm^{-1} are assigned to $\nu(\text{XeC})$ and $\nu(\text{IC})$, which are strongly coupled to C–F and C–C stretches. In contrast, the frequencies corresponding to C–C stretching and C–C stretching modes coupled to C–F modes occur at 1157–1665 cm^{-1} in C_6F_6 .²¹ These bands were calculated at 772 [779] ($[\text{C}_6\text{F}_5\text{Xe}]^+$) and 818 [829] ($\text{C}_6\text{F}_5\text{I}$) cm^{-1} , respectively, and were predicted to be intense in the infrared spectra, in agreement with the very strong band observed at 808 cm^{-1} in the infrared spectrum of $\text{C}_6\text{F}_5\text{I}$.^{22–24} This frequency was previously reported for the Cl (885 cm^{-1})^{22–24} and Br (836 cm^{-1})^{22–24} analogues, and is one of four bands that are expected to display significant mass dependencies (Table S1). In the prior studies, the 885 (Cl), 836 (Br), and 808 (I) cm^{-1} bands were assigned to pure Cl–C, Br–C, or I–C stretches most likely because of their strong intensities in their infrared spectra. The present study, however, reveals that the Xe–C and I–C stretching modes also contribute to the most intense Raman bands at 205 ($[\text{BF}_4]^-$), 201 ($[\text{B}(\text{CN})_4]^-$), and 204 cm^{-1} ($\text{C}_6\text{F}_5\text{I}$) by coupling to an in-plane CCF bending mode of the C_6F_5 ring. These coupled modes were calculated at 188 [193] and 204 [209] cm^{-1} for $[\text{C}_6\text{F}_5\text{Xe}]^+$ and $\text{C}_6\text{F}_5\text{I}$, respectively, and are predicted to be intense in their Raman spectra. The calculated and experimental frequencies provided in the present work parallel the anticipated bond

(16) Enjalbert, R.; Galy, J. *Acta Crystallogr.* **2002**, *58B*, 1005–1010.

(17) Emara, A. A. A.; Schrobilgen, G. J. *J. Chem. Soc., Chem. Commun.* **1987**, 1644–1646.

(18) Fir, B. A. *Master of Science Dissertation*, McMaster University, Hamilton, Ontario, Canada, 1999.

(19) Bates, J. B.; Quist, A. S. *Spectrochim. Acta* **1975**, *31A*, 1317–1327.

(20) Steele, D.; Whiffen, D. H. *Spectrochim. Acta* **1960**, *17*, 368–375.

(21) Steele, D.; Whiffen, D. H. *Trans. Faraday Soc.* **1959**, *55*, 369–376.

(22) Long, D. A.; Steele, D. *Spectrochim. Acta* **1963**, *19*, 1947–1954.

(23) Long, D. A.; Steele, D. *Spectrochim. Acta* **1963**, *19*, 1955–1961.

(24) Hyams, I. J.; Lippincott, E. R. *Spectrochim. Acta* **1966**, *22*, 695–702.

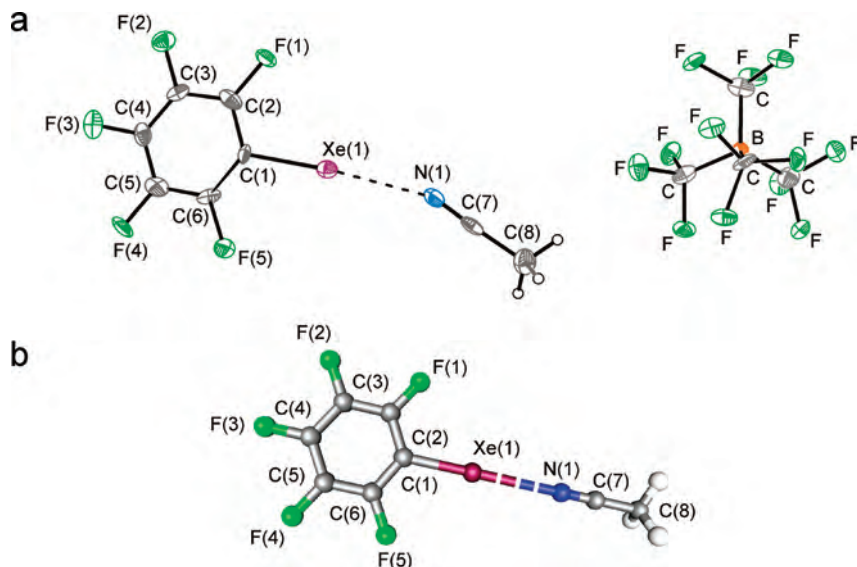


Figure 2. (a) Crystal structure of $[C_6F_5XeNCCH_3][B(CF_3)_4]$ where thermal ellipsoids are shown at the 50% probability level; (b) calculated geometry for $[C_6F_5XeNCCH_3]^+$ (SVWN/(SDB)-cc-pVTZ).

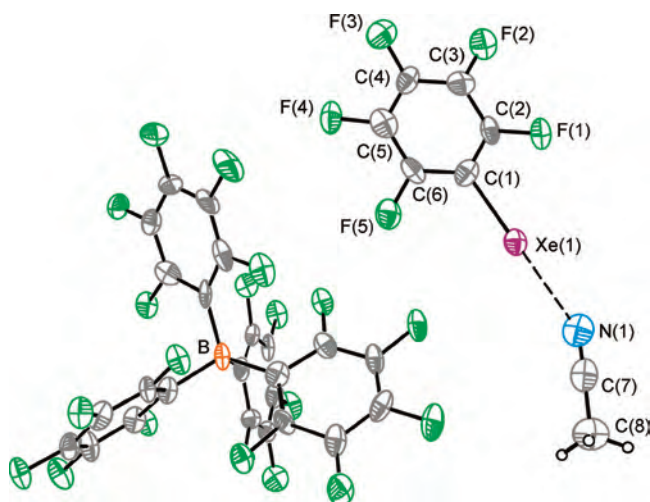


Figure 3. Crystal structure of $[C_6F_5XeNCCH_3][B(C_6F_5)_4]$ where thermal ellipsoids are shown at the 50% probability level.

strength trends for a series of xenon(II) cations in which xenon is bonded to a second row element: $\nu(XeC)$ (201, 205 cm^{-1} , $[C_6F_5Xe]^+$) < $\nu(XeN)$ (224 cm^{-1} , $[F_5SN(H)Xe]^+$)²⁵ < $\nu(XeO)$ (491 cm^{-1} , $[XeOTeF_5]^+$)²⁶ < $\nu(XeF)$ (608, 610 cm^{-1} ; $[XeF]^+$).²⁷ The bands at 106, 119 ($[BF_4]^-$); 85, 122, 126 ($[B(CN)_4]^-$); and 110, 114 (C_6F_5I) cm^{-1} are assigned to the $\delta(CCXe)$ and $\delta(CCI)$ out-of-plane and in-plane deformation modes, respectively, coupled to out-of-plane and in-plane $\delta(CCF)$ deformation modes, which are in good agreement with the calculated values of 77 [81], 112 [122] ($[C_6F_5Xe]^+$) and 80 [82], 124 [133] (C_6F_5I) cm^{-1} . The calculated trends (cm^{-1}) for the $\delta(CCX)_{oop}$ and $\delta(CCX)_{ip}$ modes (cm^{-1}) are as follows: H (804, 1142) [855, 1179] > F (135, 251) [138, 268] > Cl (107, 191) [109, 135] > Br (90, 147) [92, 134] > I (80, 124) [82, 133] > Xe (77, 112) [81, 122].

Both coupled modes involving Xe–C stretching components are predicted to shift to higher frequency by 19 [23]

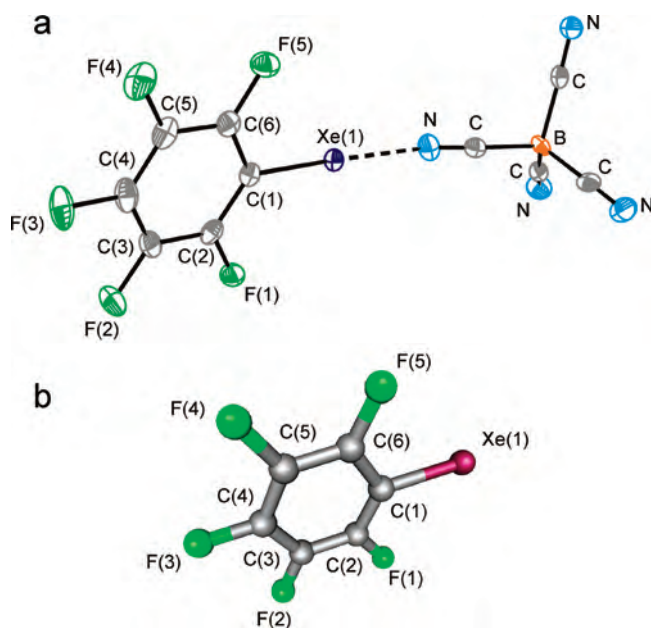


Figure 4. (a) Crystal structure of $[C_6F_5Xe][B(CN)_4]$ where thermal ellipsoids are shown at the 50% probability level; (b) calculated geometry for $[C_6F_5Xe]^+$ (SVWN/(SDB)-cc-pVTZ).

and 15 [8] cm^{-1} upon coordination but, in practice, they are observed at nearly the same frequencies in the $[C_6F_5Xe]^+$ salts (794, 795 and 201, 205 cm^{-1}) and $[C_6F_5XeNCCH_3]^+$ salts (795, 796 and 202, 203 cm^{-1}). The insensitivity of these modes to coordination is in accord with the insensitivity of the $[C_6F_5Xe]^+$ geometrical parameters to coordination (see X-ray Crystal Structures). The C–N stretch is predicted to shift by 10 [7] cm^{-1} upon coordination, which is less than the observed shift (CH_3CN , 2248 cm^{-1} ; $[C_6F_5XeNCCH_3][B(C_6F_5)_4]$, 2273 cm^{-1} ; $[C_6F_5XeNCCH_3][B(CF_3)_4]$, 2278 cm^{-1}), but is consistent with a weak donor–acceptor interac-

(25) Smith, G. L.; Mercier, H. P. A.; Schrobilgen, G. J. *Inorg. Chem.* **2008**, in press [DOI: ic702039f].

(26) Fir, B.; Whalen, J. M.; Mercier, H. P. A.; Sanders, J. C. P.; Dixon, D. A.; Schrobilgen, G. J. *J. Fluorine Chem.* **2001**, *110*, 89–107.

(27) Smith, G. L.; Mercier, H. P. A.; Schrobilgen, G. J. *Inorg. Chem.* **2007**, *46*, 1369–1378.

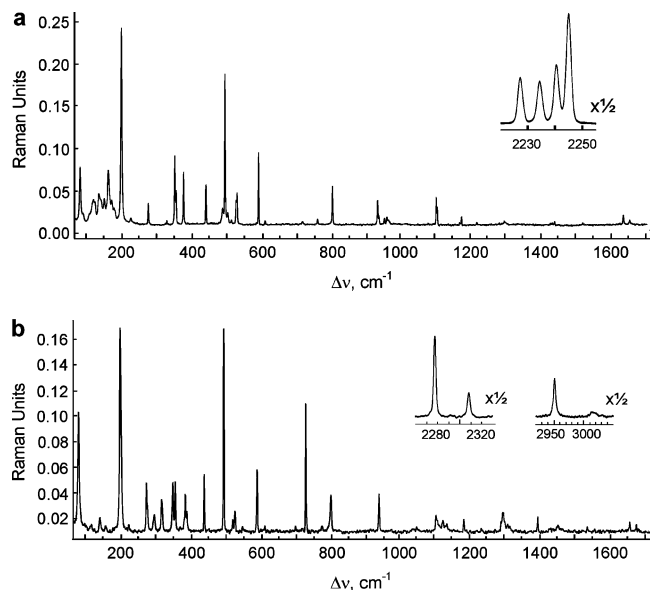


Figure 5. Raman spectra ($-150\text{ }^{\circ}\text{C}$, 1064-nm excitation) of (a) $[\text{C}_6\text{F}_5\text{Xe}][\text{B}(\text{CN})_4]$ and (b) $[\text{C}_6\text{F}_5\text{XeNCCH}_3][\text{B}(\text{CF}_3)_4]$.

tion (vide supra). The weak interaction is also supported by the calculated low frequency for the Xe–N stretch (154 [141] cm^{-1}). This frequency is significantly lower than those assigned for more covalent or stronger donor–acceptor Xe–N bonds, for example, $[\text{FXeNCH}]^+$, 330 cm^{-1} ;^{17,28} $[\text{FXeNCCH}_3]^+$, $268, 284, 288\text{ cm}^{-1}$;¹⁸ $[\text{FXeNSF}_3]^+$, 194 cm^{-1} .²⁷ The experimental frequency at 144 cm^{-1} ($[\text{B}(\text{CF}_3)_4]^-$) may be tentatively assigned to both $\nu(\text{XeN})$ and/or $\delta(\text{CCF})_{\text{ip}} + \delta(\text{CXeN})_{\text{ip}}$, because of the similarity of the calculated frequencies for both modes (Table 4) using SVWN and PBE1PBE (values in square brackets) methods. The in-plane and out-of-plane $\delta(\text{CXN})$ and $\delta(\text{XNC})$ deformation modes are calculated at 142 [134], 166 [168] cm^{-1} and 71 [74], 86 [87], 121 [113] cm^{-1} , respectively, and are coupled with in-plane and out-of-plane $\delta(\text{CCF})$ deformation modes.

(b) $[\text{BY}_4]^-$ Anions. The vibrational frequencies of $[\text{B}(\text{CN})_4]^-$,¹² $[\text{BF}_4]^-$,¹⁹ and $[\text{B}(\text{CF}_3)_4]^-$ ⁹ are in agreement with those reported earlier; their assignments have therefore been made by comparison with the published assignments, and they are not discussed further for the $[\text{BF}_4]^-$ and $[\text{B}(\text{CF}_3)_4]^-$ salts (Tables 3 and 4, footnotes c and b, respectively).

(i) $[\text{B}(\text{CN})_4]^-$. The $[\text{B}(\text{CN})_4]^-$ anion is weakly coordinated through a single nitrogen atom in the crystal structure of $[\text{C}_6\text{F}_5\text{Xe}][\text{B}(\text{CN})_4]$ (see X-ray Crystal Structures). There are four well-resolved bands in the C–N stretching region whose frequencies are in close agreement with the previously reported frequencies of the $\nu_1(\text{A}_1)$ and $\nu_6(\text{T}_2)$ C–N stretching modes of $[\text{B}(\text{CN})_4]^-$.¹² The four bands are interpreted in terms of a slightly distorted $[\text{B}(\text{CN})_4]^-$ anion having local C_{3v} symmetry in which the A_1 and T_2 symmetries under T_d symmetry correlate to A_1 and $\text{A}_1 + \text{E}$ symmetries, respectively, under C_{3v} symmetry. The symmetries of the C–N stretches of the three uncoordinated CN groups are reduced

to A symmetries under the crystal site symmetry, C_1 , resulting in removal of the E-degeneracy and the appearance of three bands in the Raman spectrum. The fourth C–N stretching band arises from the unique CN ligand coordinated to the $[\text{C}_6\text{F}_5\text{Xe}]^+$ cation. Additionally, a factor-group analysis that treats only the C–N stretching modes was carried out (Table S4). Although the analysis indicates that four additional splittings should be observed on each Raman and infrared band, these splittings and associated couplings within the unit cell are too small to be resolved in the Raman spectrum. Unlike the C–N stretches, the B–C stretches can be assigned under T_d symmetry, with only $\nu_7(\text{T}_2)$ showing a splitting (2 cm^{-1} ; see Table 3, footnote b).

(ii) $[\text{B}(\text{C}_6\text{F}_5)_4]^-$. Although $[\text{B}(\text{C}_6\text{F}_5)_4]^-$ has been widely exploited as a weakly coordinating anion,²⁹ no detailed vibrational data and assignments appear to be available for this anion. The experimental spectra of $[\text{B}(\text{C}_6\text{F}_5)_4]^-$ in the $[\text{C}_6\text{F}_5\text{XeNCCH}_3]^+$ (Figure S1) and Cs^+ (Figure S2) salts were therefore assigned by comparison with the frequencies calculated from the optimized anion geometry using the SVWN method (Tables 4 and S5 and Figure S3). There is good overall agreement between the calculated and experimental frequencies. The bands at 822 and 824 cm^{-1} are assigned to the symmetric BC_4 stretch, which is expected to be very intense in the Raman spectrum and is calculated at 837 cm^{-1} . The asymmetric BC_3 stretches are expected to occur at higher frequency, that is, $940, 986\text{ cm}^{-1}$, but only one band is observed at 978 cm^{-1} . Lower frequency modes are calculated at 600 and 609 cm^{-1} which are best described as coupled $\delta(\text{CCC})_{\text{oop}}$ and $\nu_{\text{as}}(\text{BC}_3)$ modes, but they were not observed in accord with their calculated very low intensities. The out-of-phase $[\delta(\text{BC}_2) - \delta(\text{BC}_2)]$ mode is coupled to the $\delta(\text{CCC})_{\text{oop}}$ bending mode and is assigned to the band observed at 684 cm^{-1} (calcd, 673 cm^{-1}). The in-phase $[\delta(\text{BC}_2) + \delta(\text{BC}_2)]$ mode is coupled to the $\delta(\text{CCC})_{\text{oop}}$ bending mode and is assigned to the band at 400 cm^{-1} (calcd, 409 cm^{-1}). The BC_2 rocking modes occur at 358 cm^{-1} and are in good agreement with the calculated value of 364 cm^{-1} . The remaining medium intensity bands at $574, 758, 769,$ and 776 cm^{-1} are BC_2 wagging modes that are strongly coupled to ring bending modes, $\delta(\text{CCC})_{\text{oop}}$ or $\delta(\text{CCC})_{\text{ip}}$. These modes are calculated at $578, 749, 765,$ and 775 cm^{-1} , respectively.

Computational Results. The electronic structures of the $[\text{C}_6\text{F}_5\text{Xe}]^+$ cation and the $[\text{C}_6\text{F}_5\text{XeNCCH}_3]^+$ adduct-cation were calculated using pure density functional theory (DFT) methods and (SDB-)cc-pVTZ basis sets starting from C_s and C_1 symmetries, respectively. All calculations resulted in stationary points with all frequencies real. Although the $[\text{C}_6\text{F}_5\text{Xe}]^+$ cation^{4,30,31} and CH_3CN ^{31,32} molecule had previously been the subject of theoretical calculations, they were recalculated under the same conditions as for $[\text{C}_6\text{F}_5\text{XeNCCH}_3]^+$ to confirm the experimental changes that

(28) Emara, A. A. A.; Schrobilgen, G. J. *Inorg. Chem.* **1992**, *31*, 1323–1332.

(29) Piers, W. E.; Chivers, T. *Chem. Soc. Rev.* **1997**, *26*, 345–354.
 (30) Frohn, H.-J.; Theißen, M. *Angew. Chem., Int. Ed.* **2000**, *39*, 4591–4593. ; *Angew. Chem.* **2000**, *112*, 4762–4764.
 (31) Semenov, S. G.; Sigolaev, Yu. F. *Russ. J. Org. Chem. (Transl.)* **2004**, *40*, 1835–1837; *Zh. Org. Khim.* **2004**, *40*, 1880–1881.
 (32) Alia, J. M.; Edwards, H. G. M. *J. Phys. Chem. A* **2005**, *109*, 7977–7987.

Table 3. Raman Frequencies and Intensities for $[C_6F_5Xe]^+$ in $[C_6F_5Xe][B(CN)_4]$ and $[C_6F_5Xe][BF_4]$,^a and Calculated Vibrational Frequencies, Intensities, and Assignments for $[C_6F_5Xe]^+$

[B(CN) ₄] ^{-b}	[BF ₄] ^{-c}	calcd ^d		assgnts (C _{2v}) ^e
		SVWN	PBE1PBE	
1651(5)	1659(10)	1671(5) [5]	1700(5) [4]	} v(C–C)
1632(7)	1637(15)	1620(6) [13]	1655(7) [15]	
	1523(9)	1565(<0.1) [452]	1588(<0.1) [466]	} v(C–C) / v(C–F)
		1559(1) [295]	1577(3) [312]	
1435(5)	1425(9)	1467(2) [5]	1481(4) [1]	} v(C–C)
		1376(1) [35]	1345(1) [5]	
1289(5)	1286(9)	1331(3) [7]	1338(<1) [30]	} v(C–C) / v(C–F)
1166(6)	1163(12)	1225(3) [1]	1231(2) [1]	
1096(10)	1090(9),br	1123(2) [58]	1134(2) [66]	} v(C–C) / v(C–F)
1093(14)				
924(13)	957(12)	1033(<1) [127]	1042(<1) [151]	} v(Xe–C) – (v(C–C) / v(C–F))
794(18)	795(14)	772(<1) [87]	779(1) [103]	
753(5)		752(<0.1) [<1]	770(<0.1) [<1]	} δ(CCC) _{ip}
711(4)	709(8),br	695(<0.1) [<1]	726(<0.1) [0]	
		646(<0.1) [0]	670(<0.1) [1]	} δ(CCC) _{oop}
605(5)	605(10)	591(2) [1]	618(1) [1]	
587(32)	588(61)	587(14) [5]	597(13) [4]	} δ(CCC) _{ip}
511(5)				
500(8)		489(10) [6]	497(10) [8]	} δ(CCC) _{ip}
492(62)	494(76)			
438(19)	440(35)	425(3) [<0.1]	438(3) [<0.1]	} δ(CCF) _{ip}
376(24)	382(32)			
355(17)	374(12)	344(3) [2]	352(3) [3]	} δ(CCF) _{ip}
351(30)				
		302(<1) [3]	347(3) [3]	} δ(CCC) _{oop}
		299(3) [0]	333(1) [3]	
		296(0) [<1]	309(<0.1) [1]	} δ(CCF) _{oop}
276(12)	277(20)	263(<1) [<0.1]	277(<1) [0]	
		256(<<1) [<1]	275(<1) [<1]	} δ(CCF) _{ip}
		197(<1) [1]	208(<0.1) [2]	
201(80)	205(100)	188(5) [<1]	193(5) [1]	} δ(CCF) _{oop}
173(13)				
164(25)		160(0) [<1]	164(<0.1) [<0.1]	} v(Xe–C) _{ip} + δ(CCF) _{ip}
152(13)	142(13)			
137(15)		129(<0.1) [<1]	133(<0.1) [0]	} δ(CCF) _{oop}
126(12)				
122(13)	119(12)	112(<1) [<1]	122(1) [1]	} δ(CCF) _{ip} + δ(CCXe) _{ip}
	106(15)			
85(26)		77(<1) [0]	81(<1) [<1]	} δ(CCF) _{oop} + δ(CCXe) _{oop}
55(4)	59(9)			
47(4)				lattice modes

^a Raman spectra were recorded at –150 °C in 5-mm o.d. Pyrex precision glass NMR tubes using 1064-nm excitation. Frequencies are given in cm⁻¹, and relative Raman intensities are given in parentheses. ^b Bands at 2245(100) [ν_{CN} , $\nu_1(A_1)$], 2240(54), 2234(41), 2227(44) [ν_{CN} , $\nu_6(T_2)$], 951(6), 944(6) [ν_{BC} , $\nu_7(T_2)$], 526(16), 524(13) [ν_{BCN} , $\nu_3(E)$], 486(10) [ν_{BC} , $\nu_2(A_1)$], 329(5) [ν_{BCN} , $\nu_5(T_1)$], and 143(14) [ν_{CBC} , $\nu_9(T_2)$] cm⁻¹ were assigned to $[B(CN)_4]^-$ by comparison with those given for $K[B(CN)_4]$ in ref 12. ^c Bands at 1107(11) [ν_{BF} , $\nu_3(T_2)$], 760(32) [ν_{BF} , $\nu_1(A_1)$], 524(10), 518(9) [$\nu_4(T_2)$], and 363(14), 354(59) [$\nu_2(E)$] cm⁻¹ were assigned to $[BF_4]^-$ by comparison with previous assignments given in ref 19. ^d SVWN/(SDB)-cc-pVTZ and PBE1PBE/(SDB)-cc-pVTZ; calculated infrared intensities, in km mol⁻¹, are given in square brackets and calculated Raman intensities, in Å⁴ amu⁻¹, are given in parentheses. The entry, <1, denotes an intensity that is 0.1–1.0. ^e The deformation modes of the C₆F₅ ring are denoted by δ and are relative to the plane of the C₆F₅ ring; ip and oop denote in-plane and out-of-plane, respectively.

were observed upon coordination of CH₃CN to $[C_6F_5Xe]^+$. Moreover, the previous calculations for $[C_6F_5Xe]^+$ were at a lower level [B3LYP/6–311G(3df,p) and B3LYP/6–311G(3d)] and did not provide vibrational frequencies and intensities. The present study takes into account relativistic effects by employing semirelativistic effective core potentials (RLC ECP), which was not the case in the earlier study. Key optimized geometric parameters for $[C_6F_5Xe]^+$ (C_s) and $[C_6F_5XeNCCH_3]^+$ (C₁) are listed in Table 2. The isoelectronic systems, C₆F₅X (X = Cl, Br, I), were also calculated.

There is good overall agreement between the observed and the calculated bond lengths and bond angles. The

calculations also show that the Xe–C bond is expected to elongate slightly upon coordination to nitrogen. The Xe---N distance is slightly underestimated. The calculated C–Xe---N angle (179.9°) differs from the observed C–Xe---N angles (174.9(2)° and 176.9(3)°), suggesting that the angle distortion at nitrogen arises from packing effects. Such deviations from the ideal 180° angle about Xe(II) have been encountered for RCN bases¹⁸ and F₃SN²⁷ coordinated to $[FXe]^+$. The deformability of this angle is also reflected in the low-frequencies calculated for the C–Xe---N in-plane and out-of-plane bending modes (Table 4). The Xe(1)–C(1) and N(1)–C(7) bond orders

Table 4. Raman Frequencies for $[\text{C}_6\text{F}_5\text{XeNCCH}_3][\text{B}(\text{C}_6\text{F}_5)_4]$ and $[\text{C}_6\text{F}_5\text{XeNCCH}_3][\text{B}(\text{CF}_3)_4]$ and Calculated Frequencies for $[\text{C}_6\text{F}_5\text{XeNCCH}_3]^+$, CH_3CN , and $[\text{B}(\text{C}_6\text{F}_5)_4]^-$

exptl ^a			calcd ^b				assgnts ^c
$[\text{B}(\text{CF}_3)_4]^-$ salt ^c	$[\text{B}(\text{C}_6\text{F}_5)_4]^-$ salt	CH_3CN ^d	$[\text{C}_6\text{F}_5\text{XeNCCH}_3]^+$		CH_3CN		
			SVWN	PBE1PBE	SVWN	PBE1PBE	
3014(10)		3000(38)	3064(94) [15]	3154(80) [4]	3063(65)[<1]	3148(60) [<1]	} $\nu_{\text{as}}(\text{CH}_3)$
2951(40)	2947(47) ^f	2938(94)	3061(95) [15]	3154(79) [4]	2981(186)[<1]	3067(169) [2]	
2309(28)	2303(21)		2978(384) [33]	3068(287) [10]			$\nu(\text{C}\equiv\text{N})$
2278(79)	2273(48)	2248(100)	2342(462) [244]	2400(318) [174]	2332(71)[14]	2393(62) [11]	} $\nu(\text{C}-\text{C})$
1654(9)	1660(26)		1666(9) [<1]	1697(6) [<1]			
1636(11)			1635(5) [9]	1668(9) [12]			} $\nu(\text{C}-\text{C}) / \nu(\text{C}-\text{F})$
1516(8)			1558(<1) [450]	1581(<1) [459]			
1433(9)			1557(1) [341]	1576(2)[344]			} $\nu(\text{C}-\text{C})$
			1456(14) [15]	1477(8) [10]			
			1387(2) [18]	1451(8) [15]	1391(8)[14]	1465(7) [11]	} CH_3 def. as
			1371(9) [18]	1451(8) [15]			
1377(13)	1376(20) ^f	1376(17)	1370(9) [18]	1398(7) [2]			} CH_3 def. s
			1331(1) [2]	1346(7) [<1]			
			1330(29) [8]	1344(1) [18]	1335(9)[10]	1401(6) [4]	} $\nu(\text{C}-\text{C}) / \nu(\text{C}-\text{F})$
1168(12)			1215(2) [1]	1223(2) [1]			
1121(10)			1123(21) [100]	1135(14) [90]			} $\rho_{\text{t}}(\text{CH}_3)$
1090(14)	1091(19)		1027(1) [142]	1047(1) [6]	999(<<1)[5]	1052(<1) [3]	
			989(1) [9]	1047(1) [6]			$\nu(\text{Xe}-\text{C}) + (\nu(\text{C}-\text{C}) / \nu(\text{C}-\text{F}))$
930(23)	930(23)	922(23)	988(2) [10]	1038(<1) [16]	959(4)[<1]	947(4) [1]	$\delta(\text{CCC})_{\text{ip}}$
795(23)	796(20)		983(12) [17]	957(14) [22]			} $\delta(\text{CCC})_{\text{oop}}$
			791(29) [34]	802(20) [65]			
			753(<0.1) [0]	772(<0.1) [<1]			} $\delta(\text{CCC})_{\text{ip}}$
			697(<0.1) [<1]	728(<0.1) [<1]			
			650(<0.1) [0]	673(<0.1) [0]			} $\delta(\text{CCC})_{\text{ip}}$
609(9)			608(1) [1]	632(1) [1]			
587(34)	584(56)		586(14) [5]	596(12) [4]			} $\delta(\text{CCN})$
493(92)	490(37)		490(25) [0]	499(22) [1]			
438(32)	438(22)		430(4) [0]	441(4) [<0.1]			} $\delta(\text{CCF})_{\text{oop}}$
389(15)	390(29)	387(15)	399(2) [0]	408(2) [1]	377(2)[<<1]	386(2) [<1]	
385(23)	358(24)		399(2) [<1]	408(3) [1]			} $\delta(\text{CCF})_{\text{ip}}$
357(29)	349(26)		347(3) [0]	375(3) [0]			
350(28)			345(11) [0]	354(11) [<1]			} $\delta(\text{CCF})_{\text{ip}}$
			331(1) [3]	353(1) [3]			
279(18)			298(<0.1) [1]	311(<0.1) [1]			} $\delta(\text{CCF})_{\text{ip}}$
275(28)	273(17)		262(4) [2]	278(3) [<1]			
			256(<0.1) [0]	275(<1) [<1]			} $\delta(\text{CCF})_{\text{ip}}$
			204(<1) [1]	214(<1) [1]			
202(100)	203(34)		203(17) [57]	201(26) [33]			} $\nu(\text{Xe}-\text{C}) + \delta(\text{CCF})_{\text{ip}}$
161(9)	164(19)		166(<0.1) [<1]	168(<0.1) [<1]			
144(12)			154(4) [10]	141(1) [2]			} $\nu(\text{Xe}-\text{N})$
			142(1) [3]	134(<1) [22]			
			130(<0.1) [0]	133(<0.1) [0]			} $\delta(\text{CCF})_{\text{ip}}$
			121(<1) [6]	113(<1) [6]			
121(9)			86(<0.1) [5]	87(<1) [7]			} $\delta(\text{XeNC})_{\text{oop}}$ + small $\delta(\text{CCF})_{\text{ip}}$
			71(1) [3]	74(1) [4]			
			31(<0.1) [<0.1]	24(<1) [2]			} $\delta(\text{XeNC})_{\text{oop}}$ - small $\delta(\text{CCF})_{\text{ip}}$
			24(2) [3]	23(1) [2]			
			24(<1) [3]	8(<0.1) [<0.1]			$\delta(\text{NCC})_{\text{oop}}$
52(9)	61(31)						$\rho_{\text{t}}(\text{CH}_3)$
							lattice modes

exptl		$[\text{B}(\text{C}_6\text{F}_5)_4]^-$	assgnts
Cs^+ salt	$[\text{C}_6\text{F}_5\text{Xe}]^+$ salt	calcd ^g	
2948(9)	2947(47) ^f		} combination bands
2552(10)			
		1666 (24) [<0.1]	} $\nu(\text{C}-\text{C})$
		1663 (30) [64]	
		1662 (18) [35]	
		1662 (18) [35]	
1647(28)		1649 (3) [5]	
		1648 (1) [7]	
		1648 (1) [7]	
		1645 (2) [<0.1]	

Table 4. Continued

exptl		$[B(C_6F_5)_4]^-$	
Cs ⁺ salt	$[C_6F_5Xe]^+$ salt	calcd ^g	assgnts
		1547 (2) [<0.1]	} v(C-C)/v(C-F)
		1543 (<1) [405]	
		1542 (<1) [213]	
		1542 (<1) [213]	
		1502 (<1) [734]	
		1502 (<1) [731]	
		1500 (<1) [58]	
		1482 (<1) [<0.1]	
		1424 (34) [<0.1]	
1387(16)	1385(17)	1421 (10) [3]	
1377(17)	1376(20) ^f	1409 (4) [14]	
	1369(19)	1409 (4) [14]	
		1390 (<1) [4]	
		1390 (<1) [7]	
		1390 (<1) [7]	
		1385 (<1) [0]	
		1297 (8) [91]	
1270(9), br		1296 (8) [<0.1]	
		1291 (5) [24]	
		1291 (<1) [24]	} v(C-C)
		1161 (2) [5]	
		1161 (<1) [5]	
		1159 (<1) [8]	} v(C-C)/v(C-F)
		1150 (<0.1) [<0.1]	
1120(9), br		1134 (4) [349]	
1091(10), br		1115 (2) [138]	
		1115 (2) [138]	
		1112 (1) [<0.1]	v(C-C)/v(C-F)
		1011 (1) [342]	} v(C-C)/v(C-F)
		1011 (1) [340]	
		1005 (1) [30]	} v(C-C)/v(C-F)
		989 (<1) [<0.1]	
978(10)		986 (2) [39]	} v _{as} (BC ₃)
		940 (<1) [<1]	
		940 (<1) [<1]	
824(34)	822(25)	837 (17) [28]	v _s (BC ₄)
776(15)		775 (1) [28]	} $\delta(CBC)_{wag} / \delta(CCC)_{oop}$
769(12)		775 (4) [28]	
758(15)		765 (1) [15]	
		749 (1) [62]	
		749 (1) [3]	} $\delta(CCC)_{ip}$
		725 (1) [<0.1]	
		714 (<1) [6]	
		714 (<1) [6]	
684(10)		673 (1) [35]	$[\delta(BC_2) - \delta(BC_2)] / \delta(CCC)$
662(10)		660 (<1) [23]	} $\delta(CCC)_{oop}$
		660 (<1) [23]	
		655 (<1) [<1]	
		655 (<1) [3]	
		655 (<1) [3]	$\delta(CBC)_{bend} / \delta(CCC)_{oop}$
		653 (~ 1) [0]	} $\delta(CBC)_{rock}$
		636 (~ 1) [<0.1]	
		609 (~ 1) [8]	} v _{as} (BC ₃) / $\delta(CCC)_{oop}$
		600 (<1) [2]	
		600 (<1) [2]	
		584 (31) [0]	} $\delta(CCC)_{ip}$
582(100)		580 (6) [3]	
		580 (6) [3]	
574(33)		578 (2) [6]	$\delta(CCC)_{ip} / \delta(CBC)_{wag}$
495(48)	494(57)	491 (24) [0]	$\delta(CCC)_{ip}$
478(54)	477(39)	473 (11) [<1]	} $\delta(CCC)_{ip} / \delta(CBC)$
		472 (~ 1) [<1]	
		469 (~ 1) [1]	
450(63)	450(41)	443 (6) [<1]	} $\delta(CCC)_{ip}$
		442 (4) [<1]	
422(61)	422(35)	442 (4) [<1]	
		441 (6) [0]	

Table 4. Continued

		[B(C ₆ F ₅) ₄]	
exptl		calcd ^g	assgnts
Cs ⁺ salt	[C ₆ F ₅ Xe] ⁺ salt		
400(28)		409 (7) [<1]	[$\delta(\text{BC}_2) + \delta(\text{BC}_2)$] / $\delta(\text{CCC})_{\text{oop}}$
393(66)	398(28)	389 (5) [1]	
	390(29)	381 (<1) [<1]	} $\delta(\text{CCC})_{\text{oop}}$
376(12)	376(21)	381 (1) [<1]	
		381 (1) [<1]	} $\delta(\text{CCC})_{\text{oop}} / \delta(\text{CBC})_{\text{bend}}$
		380 (~ 1) [<1]	
358(17)		364 (<1) [<1]	} $\delta(\text{CCC})_{\text{oop}} / \delta(\text{CBC})_{\text{rock}}$
		364 (<1) [<1]	
351(10)		355 (2) [0]	$\delta(\text{CCF})_{\text{ip}}$
		348 (<1) [8]	} $\delta(\text{CCF})_{\text{ip}} / \delta(\text{CBC})$
343(11)		339 (~ 1) [1]	
		339 (~ 1) [1]	} $\delta(\text{CCF})_{\text{ip}}$
		311 (<1) [<1]	
		310 (<0.1) [<1]	
		310 (<0.1) [<1]	
		309 (<1) [<0.1]	
		271 (<1) [0]	
		270 (<1) [<1]	
		270 (<0.1) [<1]	
		270 (<0.1) [<1]	
		258 (<0.1) [<1]	
		258 (<0.1) [<0.1]	
242(20)		258 (<1) [<1]	
		233 (<1) [3]	
		231 (<1) [0]	
		223 (<1) [1]	
		223 (<1) [1]	
		187 (<1) [<0.1]	
		177 (<1) [<1]	} $\delta(\text{CCF})_{\text{ip}}$
162(19)		176 (<0.1) [<1]	
158(21)		176 (<0.1) [<1]	} $\delta(\text{CCF})_{\text{oop}}$
		165 (<1) [<1]	
		158 (2) [0]	
		151 (<1) [<1]	
		151 (<1) [<1]	
		145 (<1) [<0.1]	
		144 (<1) [<0.1]	
		143 (<1) [<1]	
		136 (<0.1) [0]	
		131 (<1) [0]	
		127 (<1) [0]	} $\delta(\text{C}_6\text{F}_5)_{\text{rings}}$
		123 (<1) [<1]	
		114 (<1) [<1]	
		113 (<1) [<1]	
57(13)	61(31)	60 (2) [<0.1]	
		49 (<1) [<0.1]	
		48 (<1) [<0.1]	
		41 (~ 1) [<1]	
		41 (~ 1) [<1]	
		33 (<0.1) [<0.1]	
		29 (1) [0]	
		27 (3) [<0.1]	
		26 (<1) [0]	

^a Raman spectra were recorded at -150°C in 5-mm o.d. Pyrex precision glass NMR tubes. Frequencies are given in cm^{-1} , and relative Raman intensities are given in parentheses. ^b SVWN/(SDB)-cc-pVTZ and PBE1PBE/(SDB)-cc-pVTZ; calculated infrared intensities, in km mol^{-1} , are given in square brackets, and calculated Raman intensities, in $\text{\AA}^4 \text{amu}^{-1}$, are given in parentheses. ^c Bands at 1293(9) [$\nu(\text{B}^{10}\text{BCF}_3)$; $\nu_1(\text{A})$ and $\nu_9(\text{T})$], 1279(15) [$\nu(\text{B}^{11}\text{BCF}_3)$; $\nu_1(\text{A})$ and $\nu_9(\text{T})$], 1110(11) [$\nu(\text{CF}_3)$, $\nu_5(\text{E})$], 1034(8) [$\nu(\text{CF}_3)$, $\nu_{11}(\text{T})$], 724(65) [$\delta(\text{CF}_3)$, $\nu_2(\text{A})$], 696(8) [$\delta(\text{CF}_3)$, $\nu_{13}(\text{T})$], 546(8) [$\delta(\text{CF}_3)$, $\nu_6(\text{E})$], 525(15) [$\delta(\text{CF}_3)$, $\nu_{14}(\text{T})$], 519(11) [$\delta(\text{CF}_3)$, $\nu_{15}(\text{T})$], 318(21) [$\rho(\text{CF}_3)$, $\nu_7(\text{E})$], 298(14) [$\rho(\text{CF}_3)$, $\nu_{16}(\text{T})$], 226(9) [$\rho(\text{CF}_3)$, $\nu_{17}(\text{T})$], and 52(9) [$\tau(\text{CF}_3)$, $\nu_{19}(\text{T})$] cm^{-1} were assigned to [B(CF₃)₄]⁻ by comparison with previous assignments given in ref 9. ^d Calculated geometrical parameters: (SVWN) N–C, 1.155 Å; C–C, 1.433 Å; C–H, 1.099 Å; $\angle\text{NCC}$, 180° ; $\angle\text{CCH}$, 110.5° ; $\angle\text{HCH}$, 108.4° ; (PBE1PBE) N–C, 1.149 Å; C–C, 1.450 Å; C–H, 1.090 Å; $\angle\text{NCC}$, 180° ; $\angle\text{CCH}$, 110.1° ; $\angle\text{HCH}$, 108.9° . The entry, <1 , denotes an intensity that is 0.1–1.0. ^e The C₆F₅ ring deformation modes are denoted by δ and are relative to the plane of the C₆F₅ ring; ip and oop denote in-plane and out-of-plane, respectively. ^f Anion and cation modes overlap. ^g SVWN/cc-pVTZ.

decrease slightly upon complexation, and that of C(7)–C(8) increases concomitantly. Coordination of CH₃CN to [C₆F₅Xe]⁺ has no significant effect on the geometric

parameters of the C₆F₅ ring. The weakness of the donor–acceptor interaction is consistent with the small Xe(1)---N(1) bond order (0.11). Upon adduct formation,

Table 5. Calculated^a Natural Atomic Charges, Mayer Bond Orders, and Mayer Natural Atomic Orbital Valencies for [C₆F₅Xe]⁺, [C₆F₅XeNCCH₃]⁺, and CH₃CN

	[C ₆ F ₅ Xe] ⁺	[C ₆ F ₅ XeNCCH ₃] ⁺	CH ₃ CN
		charge [valency]	
Xe(1)	0.90 [0.71]	0.94 [0.78]	
C(1)	-0.25 [3.10]	-0.31 [3.05]	
F(1)	-0.24 [0.83]	-0.26 [0.81]	
C(2)	0.29 [3.13]	0.30 [3.13]	
F(2)	-0.22 [0.74]	-0.23 [0.73]	
C(3)	0.30 [3.02]	0.29 [3.02]	
F(3)	-0.22 [0.74]	-0.23 [0.73]	
C(4)	0.32 [3.03]	0.31 [3.03]	
F(4)	-0.22 [0.74]	-0.23 [0.73]	
C(5)	0.30 [3.02]	0.29 [3.02]	
F(5)	-0.24 [0.83]	-0.26 [0.81]	
C(6)	0.29 [3.13]	0.30 [3.13]	
N(1)		-0.46 [2.04]	-0.31 [1.96]
C(7)		0.45 [3.01]	0.27 [3.01]
C(8)		-0.80 [3.32]	-0.79 [3.30]
H(1-3)		0.31 × 3 [0.79 × 3]	0.28 × 3 [0.79 × 3]
		bond order	
Xe(1)-C(1)	0.72	0.68	
C(1)-C(2)	1.15	1.16	
C(2)-F(1)	0.85	0.84	
C(2)-C(3)	1.11	1.12	
C(3)-F(2)	0.77	0.76	
C(3)-C(4)	1.11	1.11	
C(4)-F(3)	0.77	0.76	
C(4)-C(5)	1.11	1.11	
C(5)-F(4)	0.77	0.76	
C(5)-C(6)	1.11	1.12	
C(6)-F(5)	0.85	0.84	
C(6)-C(1)	1.15	1.16	
Xe(1)---N(1)		0.11	
N(1)-C(7)		1.91	1.95
C(7)-C(8)		1.04	1.01
C(8)-H		0.76 × 3	0.76 × 3

^a SVWN/(SDB-)cc-pVTZ.

the Xe atom becomes more positive and the N atom becomes more negative. There are no significant changes in the C and F atom charges, except for the *ipso*-C atom, which becomes more negative, and the C atom bonded to N, which becomes more positive by similar absolute amounts (-0.06 and +0.10, respectively). The smaller change for the *ipso*-C is likely less because the C₆F₅ group is able to compensate for additional electron density. The Xe valency increases only slightly and that of nitrogen decreases, in accord with the formation of a weak donor-acceptor bond.

The gas-phase reaction energies corresponding to Xe---N donor-acceptor bond dissociation were calculated at the MP2/(SDB-)cc-pVTZ//SVWN/(SDB-)cc-pVTZ level of theory for [C₆F₅XeNCCH₃]⁺ (96.2 kJ mol⁻¹) and [FXeNCCH₃]⁺ (210.9 kJ mol⁻¹). Under gas-phase conditions, it is clear that [FXe]⁺ is a significantly stronger Lewis acid toward CH₃CN than [C₆F₅Xe]⁺, and this trend is paralleled by the gas-phase fluoride ion dissociation energies for C₆F₅XeF (614.9 kJ mol⁻¹) and XeF₂ (996.8 kJ mol⁻¹).

Conclusions

The syntheses and solid-state structural characterizations of [C₆F₅Xe][B(CF₃)₄], [C₆F₅XeNCCH₃][B(CF₃)₄], [C₆F₅Xe][B(CN)₄], and [C₆F₅XeNCCH₃][B(C₆F₅)₄] have provided several insights into the coordination behavior of

the [C₆F₅Xe]⁺ cation in this series of weakly coordinating anion salts. Raman spectroscopic and X-ray structure determinations, complemented by electronic structure calculations, reveal that the geometry of the [C₆F₅Xe]⁺ cation is rather insensitive to CH₃CN coordination. The [B(CF₃)₄]⁻ salt displays the weakest cation-anion interaction in its crystal structure and provides the closest approximation to the [C₆F₅Xe]⁺ cation in the gas-phase for the two unsolvated [C₆F₅Xe]⁺ salts examined in this study. The formation of the [C₆F₅XeNCCH₃]⁺ salts of the [B(C₆F₅)₄]⁻ and [B(CF₃)₄]⁻ anions is consistent with their weakly coordinating natures, allowing CH₃CN to compete effectively with these anions for the Lewis acidic xenon center of the cation. In contrast, the interaction is apparently sufficiently strong to prevent CH₃CN coordination in the [B(CN)₄]⁻ salt. Although the geometric parameters of the [B(CN)₄]⁻ anion are apparently insensitive to coordination of a single CN group to xenon, the interaction is detectable in the C-N stretching region of [B(CN)₄]⁻.

Experimental Section

[C₆F₅Xe][B(CF₃)₄] (1), [C₆F₅XeNCCH₃][B(C₆F₅)₄] (2), [C₆F₅XeNCCH₃][B(CF₃)₄] (3), and [C₆F₅Xe][B(CN)₄] (4). The metatheses of [C₆F₅Xe][BF₄] with M[BY₄] are described in detail in ref 8. In a typical synthesis, equimolar amounts of M[BY₄] and [C₆F₅Xe][BF₄] (~0.5 mmol) were dissolved in CH₃CN (each 300 μL) and combined at room temperature. The suspension was cooled

to $-40\text{ }^{\circ}\text{C}$ and centrifuged at this temperature. The mother liquor was separated, and the solid residue was washed with cold CH_3CN . The solvent was then removed under dynamic vacuum (10^{-3} mbar) at room temperature. The pale yellow solids were pumped under vacuum (10^{-3} mbar) for more than 12 h at $20\text{ }^{\circ}\text{C}$. The $[\text{C}_6\text{F}_5\text{Xe}][\text{B}(\text{CF}_3)_4]$, $[\text{C}_6\text{F}_5\text{Xe}][\text{B}(\text{CN})_4]$, and $[\text{C}_6\text{F}_5\text{XeNCCH}_3][\text{B}(\text{C}_6\text{F}_5)_4]$ salts were obtained in essentially quantitative yields. It is important to note that $[\text{C}_6\text{F}_5\text{Xe}][\text{B}(\text{CF}_3)_4]$ has a tendency to retain CH_3CN even after pumping under vacuum. It is only after repeated dissolutions ($\times 5$) in CH_2Cl_2 and evaporation under dynamic vacuum that $[\text{C}_6\text{F}_5\text{Xe}][\text{B}(\text{CF}_3)_4]$ was obtained free of CH_3CN (monitored by Raman and ^1H NMR spectroscopies). Applying this procedure to the salt containing the $[\text{B}(\text{C}_6\text{F}_5)_4]^-$ anion, $[\text{C}_6\text{F}_5\text{Xe}][\text{B}(\text{CF}_3)_4]$ was obtained.⁸ The CH_3CN -free salts were stable indefinitely at ambient temperatures in the inert atmosphere of a drybox.

Raman Spectroscopy. (a) Raman Sample Preparation. In the drybox, freshly prepared $[\text{C}_6\text{F}_5\text{Xe}]^+$ and $[\text{C}_6\text{F}_5\text{XeNCCH}_3]^+$ salts were transferred into 5-mm o.d. Pyrex precision glass NMR tubes (Wilmad 507) fused to $1/4$ -in. o.d. lengths of glass tubing which were attached to J. Young Teflon/glass stopcocks by means of $1/4$ -in. stainless steel Swagelok Ultra-Torr unions. The tubes had been previously dried under dynamic vacuum (10^{-3} mbar) at ambient temperature for at least 12 h and backfilled with dry argon prior to use. To prevent dispersion of the solid over the walls of the NMR tube, the solid material was loaded into the tube using a solids syringe fabricated from 2-mm o.d. FEP tubing and a length of 1.5-mm o.d. a stainless steel rod that functioned as a piston. After transfer of the solid, the NMR tube was connected to a glass vacuum line, cooled to $-196\text{ }^{\circ}\text{C}$, pumped under dynamic vacuum (10^{-3} mbar), and heat sealed. The Raman spectra of the resulting pale yellow powders were acquired at $-150\text{ }^{\circ}\text{C}$. The spectra of $\text{Cs}[\text{B}(\text{C}_6\text{F}_5)_4]$ (Table 4 and Figure S2), $\text{K}[\text{B}(\text{CF}_3)_4]$, CH_3CN , and CH_2Cl_2 were also measured at $-150\text{ }^{\circ}\text{C}$ for reference purposes.

(b) Raman Instrumentation and Spectral Acquisition. The low-temperature ($-150\text{ }^{\circ}\text{C}$) Raman spectra were recorded on a Bruker RFS 100 FT Raman spectrometer using 1064-nm excitation and a resolution of 1 cm^{-1} as previously described.³³ The spectra were recorded using laser powers of 100–300 mW and a total of 1500 scans.

X-ray Crystallography. (a) Crystal Growth. The following quantities of $[\text{C}_6\text{F}_5\text{Xe}]^+$ salts were weighed, in a drybox, into previously vacuum-dried $1/4$ -in. o.d. FEP T-shaped reactors, attached to Kel-F valves, and anhydrous CH_2Cl_2 was condensed onto the samples on a vacuum line: (1) $[\text{C}_6\text{F}_5\text{Xe}][\text{B}(\text{CF}_3)_4]$ (19.12 mg, 32.7 μmol ; 0.59 mL); (2) $[\text{C}_6\text{F}_5\text{XeNCCH}_3][\text{B}(\text{C}_6\text{F}_5)_4]$ (43.87 mg; 44.9 μmol ; 0.69 mL); (3) $[\text{C}_6\text{F}_5\text{Xe}][\text{B}(\text{CN})_4]$ (40.56 mg, 98.2 μmol ; 0.29 mL); (4) $[\text{C}_6\text{F}_5\text{XeNCCH}_3][\text{B}(\text{CF}_3)_4]$ (61.69 mg, 105.4 μmol ; 0.59 mL). In salts 1, 3, and 4, suspensions resulted at room temperature as well as in the case of salt 2, which was maintained at $-20\text{ }^{\circ}\text{C}$. Aliquots of CH_3CN were condensed onto the samples at $-196\text{ }^{\circ}\text{C}$ (2–4) until most (2) or all (3 and 4) of the solid material had dissolved upon warming to room temperature. The amount of CH_3CN ranged from 20–200 μL depending on the solubility of the $[\text{C}_6\text{F}_5\text{Xe}]^+$ salt. The reactors were pressurized at ~ 1 atm with dry nitrogen at $-80\text{ }^{\circ}\text{C}$ and allowed to briefly warm to room temperature to effect dissolution. Samples 1 and 2 were warmed to $\sim 30\text{ }^{\circ}\text{C}$ (≤ 10 s) to provide a near-saturated solution which was decanted into the sidearm of the reaction vessel. Upon sedimentation, the clear yellow mother liquor was decanted back into the

main arm of the reactor. The arm containing the solution was placed inside the glass Dewar of a low-temperature crystal growing apparatus³⁴ at a preset initial temperature and crystallized over several hours: (1) After 8 h at $-38\text{ }^{\circ}\text{C}$, clear, ~ 10 mm long pale yellow needles grew throughout the solution. The sample was maintained at $-40\text{ }^{\circ}\text{C}$ for an additional 26 h. (2) Clear, colorless needles grew at $-25\text{ }^{\circ}\text{C}$ throughout the solution over a period of 2 h. The temperature was maintained at $-25\text{ }^{\circ}\text{C}$ for a further 8 h. (3) After the mixture was cooled to $-8\text{ }^{\circ}\text{C}$ clear, colorless square plates grew throughout the solution. The temperature was maintained at $-8\text{ }^{\circ}\text{C}$ for ~ 20 h and was then cooled to $-20\text{ }^{\circ}\text{C}$ over a period of 2 h. (4) After 10 h at $-63\text{ }^{\circ}\text{C}$, pale yellow needle-shaped crystals grew throughout the solution. The sample was further cooled to $-66\text{ }^{\circ}\text{C}$ over a 5 h period.

The supernatants were decanted from the crystals into the sidearms of their respective reactors and were cooled to $-196\text{ }^{\circ}\text{C}$, whereupon the sidearms were heat sealed under dynamic vacuum at $-196\text{ }^{\circ}\text{C}$, and residual solvents were removed from the crystals by pumping at (1) $-67\text{ }^{\circ}\text{C}$ for 30 min, (2) $-75\text{ }^{\circ}\text{C}$ for 15–20 min, (3) $-20\text{ }^{\circ}\text{C}$ for 30 min, and (4) $-62\text{ }^{\circ}\text{C}$ for 30 min.

(b) Crystal Mounting and X-ray Data Collection. All crystals were mounted at $-110 \pm 3\text{ }^{\circ}\text{C}$ as previously described.³³ The crystals or crystal fragments used for the data acquisition had the dimensions (1) $0.26 \times 0.16 \times 0.04$ $[\text{C}_6\text{F}_5\text{Xe}][\text{B}(\text{CF}_3)_4]$; (2) $0.18 \times 0.08 \times 0.06$ $[\text{C}_6\text{F}_5\text{XeNCCH}_3][\text{B}(\text{C}_6\text{F}_5)_4]$; (3) $0.22 \times 0.12 \times 0.05$ $[\text{C}_6\text{F}_5\text{Xe}][\text{B}(\text{CN})_4]$; (4) $0.04 \times 0.04 \times 0.08$ $[\text{C}_6\text{F}_5\text{XeNCCH}_3][\text{B}(\text{CF}_3)_4]$ mm^3 .

Crystals were centered on a P4 Siemens diffractometer, equipped with a Siemens SMART 1K CCD area detector, controlled by SMART,³⁵ and a rotating anode emitting $\text{K}\alpha$ radiation monochromated ($\lambda = 0.71073\text{ \AA}$) by a graphite crystal. Diffraction data collection ($-173\text{ }^{\circ}\text{C}$) consisted of a full Ψ -rotation at $\chi = 0^{\circ}$ (using $1040 + 30$) 0.3° frames, followed by a series of short (80 frames) ω scans at various ψ and χ settings to fill the gaps. The crystal-to-detector distances were 4.970 cm for 1, 2, and 4, and 5.012 cm for 3, and the data collections were carried out in a 512×512 pixel mode using 2×2 pixel binning. Processing of the raw data was completed using SAINT+,³⁶ which applied Lorentz and polarization corrections to three-dimensionally integrated diffraction spots. The program SADABS³⁷ was used for the scaling of diffraction data, the application of a decay correction, and an empirical absorption correction on the basis of the intensity ratios of redundant reflections.

(c) Solution and Refinement of the Structure. The XPREP³⁸ program was used to confirm the unit cell dimensions and the crystal lattices. The solutions were obtained by direct methods, which located the positions of the heavy atoms. The final refinements were obtained by introducing anisotropic thermal parameters and the recommended weights for all of the atoms. The maximum electron densities in the final difference Fourier maps were located near the heavy atoms. All calculations were performed using the SHELXTL-plus package³⁸ for the structure determination and solution refinement and for the molecular graphics.

Calculations. Quantum chemical calculations were done using the program Gaussian 03 (version C.02).³⁹ Density functional theory (DFT) calculations were performed with the SVWN and

(33) Gerken, M.; Dixon, D. A.; Schrobilgen, G. J. *Inorg. Chem.* **2000**, *39*, 4244–4255.

(34) Lehmann, J. F.; Dixon, D. A.; Schrobilgen, G. J. *Inorg. Chem.* **2001**, *40*, 3002–3017.

(35) SMART, version 5.6.11; Siemens Energy and Automation, Inc.: Madison, WI, 1999.

(36) SAINT+, version 6.02; Siemens Energy and Automation, Inc.: Madison, WI, 1999.

(37) Sheldrick, G. M. SADABS (*Siemens Area Detector Absorption Corrections*), version 2.03; Bruker AXS, Inc.: Madison, WI, 1999.

PBE1PBE exchange-correlation potentials and the standard all-electron cc-pVTZ basis sets, except in the case of Xe for which the semirelativistic large core (RLC) pseudopotential basis set SDB-cc-pVTZ was used.⁴⁰ The combined use of cc-pVTZ and SDB-cc-pVTZ basis sets is indicated as (SDB)-cc-pVTZ. The geometries were fully optimized at all levels of theory using analytical gradient methods. The C–C and C–F bond lengths and frequencies of C_6F_6 were calculated for use as benchmarks.

The program GaussView⁴¹ was used to visualize the vibrational displacements that form the basis of the vibrational mode descriptions given in Tables 3, 4, S1, and S2. Natural Bond

orbital analyses were performed using SVWN densities with the NBO program.^{42–44}

Acknowledgment. We thank the Natural Sciences and Engineering Research Council of Canada (G.J.S.) and the Deutsche Forschungsgemeinschaft and the Fonds der Chemischen Industrie (H.-J.F.) for support in the form of research grants and SHARCNet (Shared Hierarchical Academic Research Computing Network; www.sharcnet.ca) for the computational resources. We also thank Prof. Helge Willner for providing samples of $K[B(CF_3)_4]$ and $K[B(CN)_4]$.

Supporting Information Available: Raman spectra of $[C_6F_5Xe][BF_4]$ and $[C_6F_5XeNCCH_3][B(C_6F_5)_4]$ (Figure S1), calculated vibrational frequencies for C_6F_5X ($X = H, F, Cl, Br, I, Xe^+$) (Table S1), calculated and experimental vibrational frequencies (Table S2) and calculated geometries (Table S3) for C_6F_5X ($X = H, F, Cl, Br, I$), Raman spectrum of $Cs[B(C_6F_5)_4]$ (Figure S2), discussion of the factor-group analysis for the distorted $[B(CN)_4]^-$ anion (also see Table S4), calculated geometries for the $[B(C_6F_5)_4]^-$ anion (Table S5 and Figure S3), and X-ray crystallographic files in CIF format for the structure determinations of $[C_6F_5Xe][B(CF_3)_4]$, $[C_6F_5XeNCCH_3][B(CF_3)_4]$, $[C_6F_5Xe][B(CN)_4]$, and $[C_6F_5XeNCCH_3][B(C_6F_5)_4]$. This material is available free of charge via the Internet at <http://pubs.acs.org>.

IC702259C

- (38) Sheldrick, G. M. *SHELXTL-Plus*, version 5.1; Siemens Analytical X-ray Instruments, Inc.: Madison, WI, 1998.
- (39) Frisch, M. J.; Trucks, G. W.; Schlegel, H. B.; Scuseria, G. E.; Robb, M. A.; Cheeseman, J. R.; Zakrzewski, V. G.; Montgomery, J. A., Jr.; Stratmann, R. E.; Burant, J. C.; Dapprich, S.; Millam, J. M.; Daniels, A. D.; Kudin, K. N.; Strain, M. C.; Farkas, O.; Tomasi, J.; Barone, V.; Cossi, M.; Cammi, R.; Mennucci, B.; Pomelli, C.; Adamo, C.; Clifford, S.; Ochterski, J.; Petersson, G. A.; Ayala, P. Y.; Cui, Q.; Morokuma, K.; Salvador, P.; Dannenberg, J. J.; Malick, D. K.; Rabuck, A. D.; Raghavachari, K.; Foresman, J. B.; Cioslowski, J.; Ortiz, J. V.; Baboul, A. G.; Stefanov, B. B.; Liu, G.; Liashenko, A.; Piskorz, P.; Komaromi, I.; Gomperts, R.; Martin, R. L.; Fox, D. J.; Keith, T.; Al-Laham, M. A.; Peng, C. Y.; Nanayakkara, A.; Challacombe, M.; Gill, P. M. W.; Johnson, B.; Chen, W.; Wong, M. W.; Andres, J. L.; Gonzalez, C.; Head-Gordon, M.; Replogle, E. S.; Pople, J. A. *Gaussian 03W*, version 6.0; Gaussian, Inc.: Pittsburgh, PA, 2003.
- (40) Basis sets were obtained from the Extensible Computational Chemistry Environment Basis set Database, version 2/25/04, as developed and distributed by the Molecular Science Computing Facility, Environmental and Molecular Science Laboratory, which is part of the Pacific Northwest Laboratory, P.O. Box 999, Richland, WA 99352.
- (41) Dennington, R. I.; Keith, T.; Millam, J. M.; Eppinnett, K.; Hovell, W. L.; Gilliland, R. *GaussView*, version 3.07; Semichem, Inc.: Shawnee Mission, KS, 2003.

- (42) Reed, A. E.; Weinstock, R. B.; Weinhold, F. *J. Chem. Phys.* **1985**, *83*, 735–746.
- (43) Reed, A. E.; Curtiss, L. A.; Weinhold, F. *Chem. Rev.* **1988**, *88*, 899–926.
- (44) Glendening, E. D.; Reed, A. E.; Carpenter, J. E.; Weinhold, F. *NBO*, version 3.1; Gaussian, Inc.: Pittsburgh, PA, 1990.